ARTICLE

Mutations in *PYCR2*, Encoding Pyrroline-5-Carboxylate Reductase 2, Cause Microcephaly and Hypomyelination

Tojo Nakayama,[1,2,3,19] Almundher Al-Maawali,[1,2,4,19] Malak El-Quessny,[1,2] Anna Rajab,[5] Samir Khalil,[6,7] Joan M. Stoler,[1,3] Wen-Hann Tan,[1,3] Ramzi Nasir,[3,8] Klaus Schmitz-Abe,[1,2,3,9] R. Sean Hill,[1,2,10] Jennifer N. Partlow,[1,2,10] Muna Al-Saffar,[1,2,10,11] Sarah Servattalab,[1,2,10] Christopher M. LaCoursiere,[12] Dimira E. Tambunan,[12] Michael E. Coulter,[1,2,10,13] Princess C. Elhosary,[1,2,10,12] Grzegorz Gorski,[14] A. James Barkovich,[15] Kyriacos Markianos,[1,2,3,9] Annapurna Poduri,[12,16,17] and Ganeshwaran H. Mochida[1,2,3,18,*]

Despite recent advances in understanding the genetic bases of microcephaly, a large number of cases of microcephaly remain unexplained, suggesting that many microcephaly syndromes and associated genes have yet to be identified. Here, we report mutations in *PYCR2*, which encodes an enzyme in the proline biosynthesis pathway, as the cause of a unique syndrome characterized by postnatal microcephaly, hypomyelination, and reduced cerebral white-matter volume. Linkage mapping and whole-exome sequencing identified homozygous mutations (c.355C>T [p.Arg119Cys] and c.751C>T [p.Arg251Cys]) in *PYCR2* in the affected individuals of two consanguineous families. A lymphoblastoid cell line from one affected individual showed a strong reduction in the amount of PYCR2. When mutant cDNAs were transfected into HEK293FT cells, both variant proteins retained normal mitochondrial localization but had lower amounts than the wild-type protein, suggesting that the variant proteins were less stable. A PYCR2-deficient HEK293FT cell line generated by genome editing with the clustered regularly interspaced short palindromic repeat (CRISPR)-Cas9 system showed that PYCR2 loss of function led to decreased mitochondrial membrane potential and increased susceptibility to apoptosis under oxidative stress. Morpholino-based knockdown of a zebrafish *PYCR2* ortholog, *pycr1b,* recapitulated the human microcephaly phenotype, which was rescued by wild-type human *PYCR2* mRNA, but not by mutant mRNAs, further supporting the pathogenicity of the identified variants. Hypomyelination and the absence of lax, wrinkly skin distinguishes this condition from that caused by previously reported mutations in the gene encoding PYCR2's isozyme, PYCR1, suggesting a unique and indispensable role for PYCR2 in the human CNS during development.

Introduction

Microcephaly is a condition in which the brain fails to achieve normal size.[1,2] The etiology of microcephaly is highly heterogeneous and includes environmental and genetic causes.[3] Underlying pathogenic mechanisms in genetic microcephaly are also diverse. Defects in centrosomes and mitotic spindles[4,5] and DNA-repair defects[6] typically manifest with microcephaly at birth (congenital microcephaly). On the other hand, degenerative conditions, including inborn errors of metabolism, are often associated with the development of microcephaly after birth (postnatal microcephaly).[1] In rare instances, microcephaly can be associated with insufficient formation of myelin, a condition known as hypomyelination.[7] Although genetic causes of many hypomyelination syndromes have recently been identified, there are still many cases with an unknown etiology.[8] The differential diagnosis of microcephaly with hypomyelination includes Pelizaeus-Merzbacher disease (MIM 312080), due to mutations in *PLP1* (MIM 300401),[9,10] and hypomyelinating leukoencephalopathy 6 (MIM 612438), due to mutations in *TUBB4A* (MIM 602662).[11] In addition, inborn errors of metabolism, such as phosphoglycerate dehydrogenase deficiency (MIM 601815)[12,13] and severe 5,10-methylenetetrahydrofolate reductase deficiency (MIM 236250),[3,14] are also important causes of microcephaly with hypomyelination.

In this study, we investigated children (from two consanguineous families) with a unique presentation of microcephaly, hypomyelination, and reduced white-matter volume and identified mutations in *PYCR2*, encoding

[1]Division of Genetics and Genomics, Department of Medicine, Boston Children's Hospital, Boston, MA 02115, USA; [2]Manton Center for Orphan Disease Research, Boston Children's Hospital, Boston, MA 02115, USA; [3]Department of Pediatrics, Harvard Medical School, Boston, MA 02115, USA; [4]Department of Genetics, College of Medicine and Health Science, Sultan Qaboos University, Muscat 123, Oman; [5]National Genetics Center, Directorate General of Health Affairs, Ministry of Health, Muscat 113, Oman; [6]Department of Pediatrics, Al-Makassed Islamic Charitable Society Hospital, Jerusalem 91220; [7]Faculty of Medicine, Al-Quds University, Jerusalem 90612; [8]Division of Developmental Medicine, Department of Medicine, Boston Children's Hospital, Boston, MA 02115, USA; [9]Program in Medical and Population Genetics, Broad Institute of MIT and Harvard, Cambridge, MA 02142, USA; [10]Howard Hughes Medical Institute, Boston Children's Hospital, Boston, MA 02115, USA; [11]Department of Paediatrics, College of Medicine and Health Sciences, United Arab Emirates University, PO Box 17666, Al-Ain, United Arab Emirates; [12]Department of Neurology, Boston Children's Hospital, Boston, MA 02115, USA; [13]Harvard-MIT Division of Health Sciences and Technology, Cambridge, MA 02139, USA; [14]Cellular Neuroscience Core, F.M. Kirby Neurobiology Center, Boston Children's Hospital, Boston, MA 02115, USA; [15]Department of Radiology and Biomedical Imaging, University of California, San Francisco, San Francisco, CA 94143, USA; [16]Epilepsy Genetics Program, Boston Children's Hospital, Boston, MA 02115, USA; [17]Department of Neurology, Harvard Medical School, Boston, MA 02115, USA; [18]Pediatric Neurology Unit, Department of Neurology, Massachusetts General Hospital, Boston, MA 02114, USA
[19]These authors contributed equally to this work
*Correspondence: ganesh.mochida@childrens.harvard.edu
http://dx.doi.org/10.1016/j.ajhg.2015.03.003.

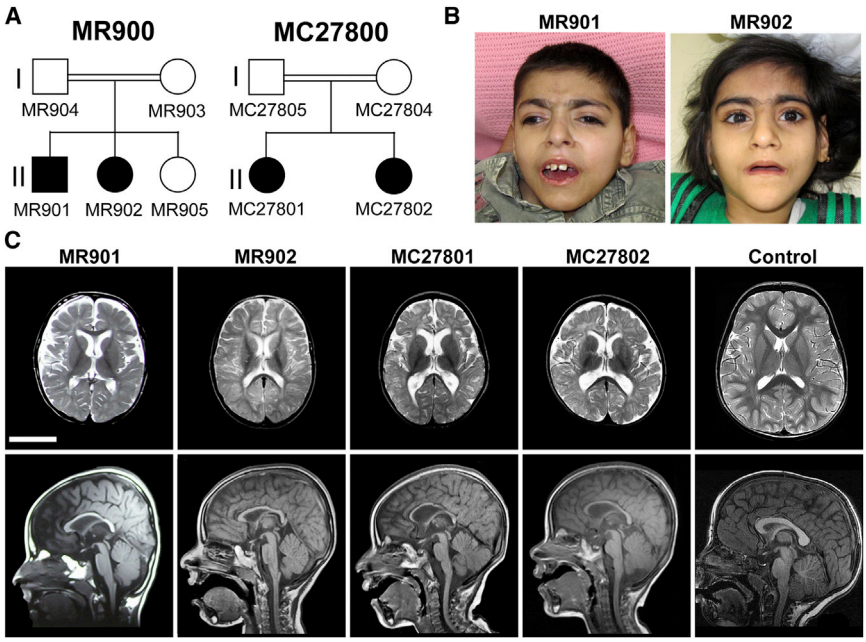

Figure 1. Pedigrees Studied and Findings from Brain MRI of the Affected Individuals

(A) Pedigree structure of the studied families (MR900 and MC27800). Shaded symbols indicate affected individuals.

(B) Facial pictures of the affected individuals in family MR900.

(C) MRI findings of the affected individuals. T2-weighted axial images (top row) and T1-weighted sagittal images (bottom row) are shown. The ages at imaging were 4 years and 0 months (MR901), 3 years and 4 months (MR902), 2 years and 7 months, (MR27801), 1 year and 10 months (MC27802), and 3 years and 1 month (control subject). All affected individuals showed microcephaly, hypomyelination, reduced white-matter volume, a thin corpus callosum, and a mildly thin brain stem. The scale bar represents 5 cm.

an enzyme in the proline biosynthesis pathway, as underlying this syndrome.

Material and Methods

Human Studies

This study was approved by the institutional review board of Boston Children's Hospital and equivalent committees of the other participating institutions. Written informed consent was obtained from all participants or their legal guardians.

Genome-wide SNP Genotyping and Linkage Analysis

Genome-wide SNP genotyping was performed for all individuals shown in Figures 1A and 1B by either the Illumina HumanOmniExpress BeadChip array (for family MC27800) or the Affymetrix Genome-Wide Human SNP Array 6.0 (for family MR900) according to the manufacturers' instructions. Combined genome-wide LOD scores for the two families were calculated with high-quality SNPs shared between the Illumina and Affymetrix arrays. PLINK[15] was used to reduce linkage disequilibrium between markers, and MERLIN[16] was used to remove genotyping errors and calculate LOD scores under the assumption of an autosomal-recessive mode of inheritance with 100% penetrance and a disease allele prevalence of 0.0001.

Whole-Exome Sequencing and Sanger Sequencing

Coding regions were captured with Illumina TruSeq enrichment (62 Mb) with sequencing on an Illumina HiSeq with 101-bp paired-end reads. Sequencing of individual MR901 yielded 14 Gb of sequencing (resulting in 20× coverage of 86.7% of the target region), and sequencing of individual MC27801 yielded 12 Gb of sequence (resulting in 20× coverage of 84.8% of the target region). Reads marked as duplicates by Picard (v.1.101) were excluded before mapping to the human genome reference sequence (GRCh37/hg19). The sequences were aligned to the reference sequence with the Burrows-Wheeler Aligner, and variants were called with mpileup (SAMtools). The Variant Explorer pipeline developed by the authors (K.S.-A and K.M.) was used for annotating all variants according to minor-allele-frequency data from the NHLBI Exome Sequencing Project Exome Variant Server (September 2013), Complete Genomics (February 2012), dbSNP (134–137), and 1000 Genomes (May 2012). Sanger sequencing of candidate variants was performed according to standard protocol. Primers were designed with Primer3, and their sequences are listed in Table S1.

RNA Sequencing

mRNA sequencing data from human fetal (Carnegie stage 18) cerebral cortex was obtained as previously described.[17]

Lymphoblastoid Cell Lines

Epstein-Barr-virus-transformed lymphoblastoid cell lines from one affected individual (MR901), his father (MR904), and one control subject were cultured in DMEM with 15% fetal bovine serum (FBS) and 1% v/v penicillin-streptomycin solution. The cell lines were grown in 5% CO_2 at 37°C. For immunoblotting, cells were extracted with M-PER mammalian protein-extraction reagent (Thermo Scientific) according to the manufacturer's protocol.

Molecular Cloning

Human *PYCR2* cDNA with no stop codon was synthesized as a double-strand genomic block (Integrated DNA Technologies) with an N-terminal overhang. The gene block was cloned into the pcDNA3.2/V5/GW-D-TOPO vector (Life Technologies) with a C-terminal V5 tag with the use of a TOPO cloning site. *PYCR2* point mutations, c.355C>T (p.Arg119Cys) and c.751C>T (p.Arg251Cys), were introduced with the QuikChange II Site-Directed Mutagenesis Kit (Agilent Technologies). For generating additional *PYCR2* cDNA constructs for immunoprecipitation, the V5 tag was replaced with an HA tag by PCR, and the product was subcloned into the pcDNA 3.1 vector (Life Technologies). For quantifying the level of exogenous PYCR2, Lipofectamin2000 (Life Technologies) was used to transfect HEK293FT cells (Invitrogen) with equal amounts of human *PYCR2* expression vectors

along with EGFP expression vector (pEGFP-C1, Clontech). The cells were cultured in DMEM with 10% FBS and 1% v/v penicillin-streptomycin solution. All cell lines were grown in 5% CO_2 at 37°C. The transfected cells were cultured for 48 hr and then analyzed by immunoblot or immunofluorescence.

Genome Editing Using the CRISPR-Cas9 System

To introduce genomic alternations at the *PYCR2* locus in the HEK293FT cell line, we performed genome editing with the clustered regularly interspaced short palindromic repeat (CRISPR)-Cas9 system.[18] A 20-nt guide RNA (gRNA) sequence (5′-GCCCT GCACTTTCTAGAGAG-3′) was designed to target double-strand breaks at *PYCR2* exon 6 and was cloned into a full U6 promoter site next to a protospacer-adjacent motif (5′-NGG-3′). pSpCas9(BB)-2A-GFP plasmids (PX459, Addgene) were cultured in lysogeny broth containing ampicillin and purified. With the Fugene HD (Promega) transfection reagent, HEK293FT cells were transfected with 1 μg of SpCas9 plasmid and 1 μg of gRNA plasmid in 6-well plates. Forty-eight hours after transfection, cells were sorted with GFP signal by fluorescence-activated cell sorting. Sorted cells were cultured in 10-cm plates until they formed single-cell colonies, which were then manually picked and cultured in 96-well dishes until they were 100% confluent. DNA was extracted from each colony (QuickExtract DNA Extraction Solution, Epicenter), and the targeted genomic region was sequenced. Primer sequences used for Sanger sequencing are listed in Table S1.

Immunofluorescence Analysis

For mitochondrial labeling, cultured cells were washed with 37°C PBS once and incubated with an X-rosamine derivative (MitoTracker, Life Technologies) at a concentration of 100 nM for 30 min without FBS. For immunofluorescence, cells were washed in PBS with glycine (PBS-G) twice. Cells were fixed in 4% (w/v) paraformaldehyde in PBS for 15 min and permeabilized with 0.1% (w/v) Triton X-100 in PBS for 5 min at room temperature. Cells were then incubated overnight at 4°C in PBS with 3% BSA and antibodies to PYCR2 (LS-C115748, LsBio) or V5 (R960-25, Life Technologies) and were visualized with immunoglobulin G Alexa Fluor 488 and 594 conjugates (Life Technologies). DNA was counterstained with Hoechst 33342, and cells were mounted in Fluoromount-G (SouthernBiotech). Images were collected with an AxioVision confocal microscope and light microscope (Zeiss) and processed with ImageJ[19] and Illustrator CS4 (Adobe Systems).

Immunoblot and Co-immunoprecipitation Analyses

For whole-cell immunoblotting, resuspended cell pellets were extracted with RIPA lysis buffer (150 mM NaCl, 0.1% Triton X-100, 0.5% sodium deoxycholate, 0.1% SDS, and 50 mM Tris-HCl [pH 8.0]) and protease inhibitors (cOmplete Mini, Roche). For subcellular fractionation, cells were washed in PBS and resuspended in isotonic mitochondria-isolation buffer (10 mM Tris/MOPS, 200 mM sucrose, and 1 mM EGTA/Tris [pH 7.4]) as previously described[20] and then homogenized by 20 strokes with a Teflon pestle in a glass potter. The suspension was centrifuged at 600 × *g* for 10 min at 4°C. The supernatant was centrifuged at 10,000 × *g* for 20 min at 4°C for separating the mitochondrial fraction (pellet) from the cytosolic fraction (supernatant). The mitochondria were washed once with the isotonic buffer, and the cytosolic fraction was centrifuged at 16,000 × *g* for 20 min at 4°C for removal of any residual mitochondria. Mitochondria were lysed in the RIPA lysis buffer with protease inhibitors.

The samples were separated on SDS-PAGE, blotted on a polyvinylidene fluoride membrane, and probed with antibodies against the following: PYCR2 (LS-C115748, LsBio; 1:200), V5 (R960-25, Life Technologies; 1:5,000), GFP (ab13970, Abcam; 1:5,000), IkBα (ab32518, Abcam; 1:1,000), VDAC1 (ab154856, Abcam; 1:1,000), β-actin (ab8227, Abcam; 1:1,000), SDHA (ab14715, Abcam; 1:1,000), and MT-CO2 (ab79393, Abcam; 1:500). Blots were scanned on a Li-Cor Odyssey imager. Signal intensities were quantified with Image Studio Lite (Li-Cor).

For co-immunoprecipitation, HEK293FT cells were transfected with one of the following combinations: (1) cDNAs encoding HA-tagged and V5-tagged wild-type PYCR2, (2) cDNAs encoding HA-tagged and V5-tagged p.Arg251Cys variant PYCR2, or (3) a control EGFP expression vector (pEGFP-C1, Clontech). After 48 hr, cells were washed once with PBS and then incubated with the chemical crosslinker dithiobis (succinimidyl propionate) (Thermo Scientific) at a 1.5 mM concentration in PBS for 30 min. The reaction was quenched with 100 mM Tris-HCl for 15 min. Cells were then lysed with RIPA lysis buffer, and small amounts of lysates were reserved as input fractions. The remaining portions of lysates were incubated with pre-washed monoclonal anti-HA agarose conjugate resin (Sigma-Aldrich) overnight on a shaker at 4°C. The resin beads were washed four times with RIPA buffer and resuspended in 2× reducing SDS sample buffer. All samples were boiled at 98°C for 10 min and then briefly vortexed, and supernatants were applied to immunoblotting. Immunoblotting was performed as described above with antibodies for HA (11867423001, Roche; 500 ng/ml), V5 (R960-25, Life Technologies; 1:1,000), and β-actin (ab8227, Abcam; 1:1,000). The experiment was repeated twice.

Apoptosis Assay

Cells were washed with 37°C PBS once and incubated with 400 μM hydrogen peroxide (H1009, Sigma-Aldrich) for 1 hr without FBS. Subsequently, medium was replaced with DMEM with 10% FBS, and cells were incubated for an additional 24 hr. Cells were then washed with PBS-G twice, fixed in 4% (w/v) paraformaldehyde in PBS for 15 min, and permeabilized with 0.1% (w/v) Triton X-100 in PBS for 5 min at room temperature. A TUNEL assay (Click-iT, Life Technologies) was performed according to the manufacturer's instruction. Cells were then stained with Hoechst 33342 and mounted in Fluoromount-G (SouthernBiotech). Images were collected with an AxioVision confocal microscope and light microscope (Zeiss) and processed with ImageJ[19] for cell counting. More than 3,000 cells were analyzed per experiment, and each experiment was repeated twice. Statistical analysis was performed with SPSS Statistics 22 (IBM).

Zebrafish Morpholino Experiments

Zebrafish were maintained according to animal research guidelines at Boston Children's Hospital. Morpholino oligonucleotides (MOs; Gene Tools) that interfere with translation of *pycr1a* (RefSeq accession number NM_200826.1) and *pycr1b* (RefSeq NM_001020618.1) by blocking the start codon were modified from previously described constructs.[21] The sequences of the designed MOs for *pycr1a* and *pycr1b* were 5′-GCTCCGATAAATCCCA CACTCATTC-3′ and 5′-GCTCCAATGAAGCCCACACTCATCC-3′, respectively. The MOs were resuspended in sterile water to a concentration of 1 mM and were further diluted to 2.5, 3.5, and 5.0 ng/μl with phenol red and water. One nanoliter of each MO solution was injected into 1- to 2-cell-stage zebrafish embryos.

Table 1. Clinical Presentation of the Affected Individuals with *PYCR2* Mutations

	Family MR900		Family MC27800	
	MR901	**MR902**	**MC27801**	**MC27802**
Parental consanguinity	yes (first cousins)	yes (first cousins)	yes (first cousins)	yes (first cousins)
Gender	male	female	female	female
Age at examination	11 years, 6 months	10 years, 3 months	9 years, 5 months	7 years, 8 months
Head circumference at birth	NA	NA	35 cm (+0.2 SD)	34 cm (−0.5 SD)
Head circumference at examination	43.6 cm (−7.0 SDs)	42.6 cm (−7.7 SDs)	44 cm (−6.6 SDs)	46 cm (−4.5 SDs)
Length	88 cm (−4.6 SDs) at 5 years, 2 months	80 cm (−4.8 SDs) at 3 year, 11 months	92 cm (−2.0 SDs) at 3 years, 11 months	83 cm (−1.3 SDs) at 2 years, 2 months
Weight	10.8 kg (−3.7 SDs) at 4 years, 6 months	8.3 kg (−4.4 SDs) at 3 years, 6 months	10 kg (−3.5 SDs) at 3 years, 11 months	9 kg (−3.0 SDs) at 2 years, 2 months
Motor development	crawled on chest but is now bedridden	sat with support and crawled at 14 months but is now mostly bedridden	does not roll over or sit unsupported	rolls over and sits with support
Speech and cognition	babbled and responded to name but now shows little response to stimuli; no words	babbled at 8 months; no words	recognizes parents with social smile; no words	recognizes parents with social smile; no words
Motor examination	severe muscle wasting, hypertonia, brisk DTRs	severe muscle wasting, hypertonia, brisk DTRs	severe muscle wasting, limited range of motion of the hips and knees, hyperextensibility of wrists and ankles, brisk DTRs	severe muscle wasting, hyperextensibility of the wrists and ankles, brisk DTRs
Facial features	down-slanting eyes, prominent eyelashes, thin vermilion of the lips	prominent eyelashes, thin vermilion of the lips	up-slanting eyes, bulbous nasal tip, protuberant ears with hypoplastic antihelix	down-slanting eyes, blunted nasal tip, prominent jaw
Other findings	exotropia, undescended testicles, type 1 diabetes, gastrostomy tube	poor dentition, malformed teeth	large atrial septal defect, gastrostomy tube	none reported
MRI Findings				
Age at MRI	4 years, 0 months	3 years, 4 months	2 years, 7 months	1 year, 10 months
Myelination	hypomyelination	hypomyelination	hypomyelination	hypomyelination
White-matter volume	markedly diminished	markedly diminished	markedly diminished	markedly diminished
Corpus callosum	thin	thin	very thin	very thin
Brain stem	thin	slightly thin	slightly thin	slightly thin

Abbreviations are as follows: DTR, deep tendon reflex; NA, not available.

A standard control MO against β-globin (Gene Tools) was used at the same concentrations and volume as those of the experimental MOs. Injected embryos and uninjected clutch-mate controls were analyzed at 0, 1, 2, 3, and 4 days post-fertilization (dpf) for survival, motility, and morphology. For the head-width measurement, 20 morphant larvae and 20 control larvae were randomly selected at 4 dpf, and the maximum head width was measured by an investigator blinded to the injection procedure. For rescue experiments, human *PYCR2* cDNA was transcribed in vitro with a T7 Kit (Ambion), and 20 pg of the resulting mRNA was co-injected with MOs.

Zebrafish Histology

For histology analysis, zebrafish embryos (4 dpf) were anesthetized on ice and fixed in modified Karnovsky fixative (2% paraformaldehyde and 2.5% glutaraldehyde in 0.1 M sodium cacodylate buffer [pH 7.4]) for 2 hr, rinsed twice in 0.1 M sodium cacodylate buffer, and incubated in 2% osmium tetroxide in 0.1 M sodium cacodylate buffer for 2 hr. After rinsing in cacodylate buffer, fish were dehydrated in a graded ethanol series and embedded in TAAB 812 Resin (Canemco & Marivac). After polymerization at 60°C, semithin sections (0.5 μm) were prepared and stained with toluidine blue. Images were collected with a light microscope (E800, Nikon) and processed with ImageJ[19] and Illustrator CS4 (Adobe Systems).

Results

Clinical Presentation

A summary of clinical findings is presented in Table 1. Family MR900 is a consanguineous Omani family with two children affected by microcephaly and intellectual disability (Figure 1A). The proband (MR901) was born at full term by spontaneous vaginal delivery. Developmental delay and hypertonia of the limbs were noted at 5 months

of age. When he was 11 months old, his occipital frontal circumference (OFC) was 42 cm (−3.3 SDs). At 1 year of age, he sat with support, crawled, and responded to his name with a social smile, but subsequently he regressed developmentally. He developed type 1 diabetes with positive anti-GAD antibody at 4 years of age and was started on insulin. At 4 years and 6 months of age, he weighed 10.8 kg (−3.7 SDs). When he was 5 years and 2 months old, his OFC was 44 cm (−5.2 SDs), and his length was 88 cm (−4.6 SDs). When he was 11 years old, his OFC was 43.6 cm (−7.0 SDs). He was cachectic and had minimal interaction with his surroundings. He had generalized hypertonia with increased deep tendon reflexes and bilateral extensor plantar responses. His plasma amino acid profile was not indicative of an inborn error of metabolism. Blood lactate and ammonia were normal. His sister (MR902) had a similar clinical course. She was born at full term after an uneventful pregnancy and delivery. Reportedly, she was doing well until 8 months of age, when she presented with anorexia and weight loss. Subsequently, she was noted to show microcephaly and global developmental delay. At 3 years and 6 months of age, she weighed 8.3 kg (−4.4 SDs). When she was 3 years and 11 months of age, her OFC was 42 cm (−4.9 SDs), and her length was 80 cm (−4.8 SDs). When she was 10 years old, her OFC was 42.6 cm (−7.7 SDs). She was cachectic and mostly bedridden and showed limited social interaction. She also had generalized hypertonia, increased deep tendon reflexes, and extensor plantar responses.

Family MC27800 is from Palestine, and similarly, two siblings presented with microcephaly and intellectual disability (Figure 1A). The proband (MC27801) was born at full term with transient fetal distress during delivery. Her OFC at birth was 35 cm (+0.2 SD). She showed general hypotonia and was slow in acquiring developmental milestones. A large atrial septal defect was surgically closed when she was 2 years old. When she was examined at 3 years and 11 months of age, her OFC was 42 cm (−4.9 SDs), her length was 92 cm (−2.0 SDs), and her weight was 10 kg (−3.5 SDs). She was not able to sit and did not speak, but she showed some social interaction. No obvious regression was noted at that time. Neurological examination was remarkable for generalized hypertonia. When she was examined at 9 years and 5 months of age, her OFC was 44 cm (−6.6 SDs). She could not roll over, sit, or speak but recognized her parents and responded by smiling or laughing. She had severe muscle wasting, and her hip and knees showed limited range of motion, but her wrist and ankle joints showed hyperextensibility. Deep tendon reflexes were increased. Her blood lactate, plasma amino acids, and urine organic acids were normal. Her sister (MC27802) was delivered at full term by Caesarean section after an uncomplicated pregnancy, and her OFC at birth was 34 cm (−0.5 SD). She presented with global developmental delay. She never achieved sitting, crawling, or standing, but no apparent regression was noted. Examination at 2 years and 2 months of age revealed an OFC of 43.2 cm (−3.1 SDs), length of 83 cm (−1.3 SDs), and weight of 9 kg (−3.0 SDs). She followed objects visually but did not speak. Neurological examination was remarkable for truncal hypotonia and appendicular hypertonia. When she was examined at 7 years and 8 months of age, her OFC was 46 cm (−4.5 SDs). She was able to roll over and sit with support but did not speak. She recognized her parents and responded by smiling or laughing. She had severe muscle wasting. Her wrist and ankle joints showed hyperextensibility, and deep tendon reflexes were increased.

There were minor facial dysmorphisms, but no consistent features among the affected individuals were noted (Figure 1B and Table 1). None of the affected individuals had notable skin findings. All affected individuals underwent brain MRI, which revealed similar features, including microcephaly with decreased cerebral white-matter volume (with associated thin corpus callosum, thin brain stem, and mild ventriculomegaly) and significant hypomyelination (Figure 1C). The cerebellum was unremarkable.

Identifying *PYCR2* Mutations by Linkage Mapping and Whole-Exome Sequencing

Because of the similar clinical presentation and consanguinity in each family, we hypothesized that the two families were affected by the same allelic autosomal-recessive condition. We performed genome-wide SNP analysis of both families and found that the four affected individuals from both families shared a genomic region of homozygosity on chromosome 1q. This was the only homozygous region shared by all affected individuals and was over 1 cM. The region was delineated by SNP markers rs2405523 and rs10802533 and was 11.6 Mb in size. The haplotypes were different between the two families. We also calculated a combined genome-wide LOD score for both families and obtained a maximum multipoint LOD score of 3.72 within the candidate region on chromosome 1q (Figure 2A). No other region in the genome had a LOD score over 1.0.

Next, we performed whole-exome sequencing on two affected individuals (MR901 and MC27801), one from each family. We filtered the identified variants for call quality, homozygosity, potential pathogenicity, population frequency, and localization within the candidate interval. Individuals MR901 and MC27801 were found to have three and two rare candidate variants, respectively (Table S2). Only one gene was shared by both individuals, and this was *PYCR2* (RefSeq NM_013328.3), which encodes pyrroline-5-carboxylate reductase 2 (PYCR2). The variants were homozygous c.355C>T (p.Arg119Cys) in individual MR901 and homozygous c.751C>T (p.Arg251Cys) in individual MC27801 (Figure 2B). The residue Arg119 is located in the NADH-binding domain, and the residue Arg251 is in the dimerization domain of PYCR2 (InterPro). We confirmed these variants by Sanger sequencing, and they segregated with the disease in each family (Figure 2C). Both variants were predicted to be damaging by

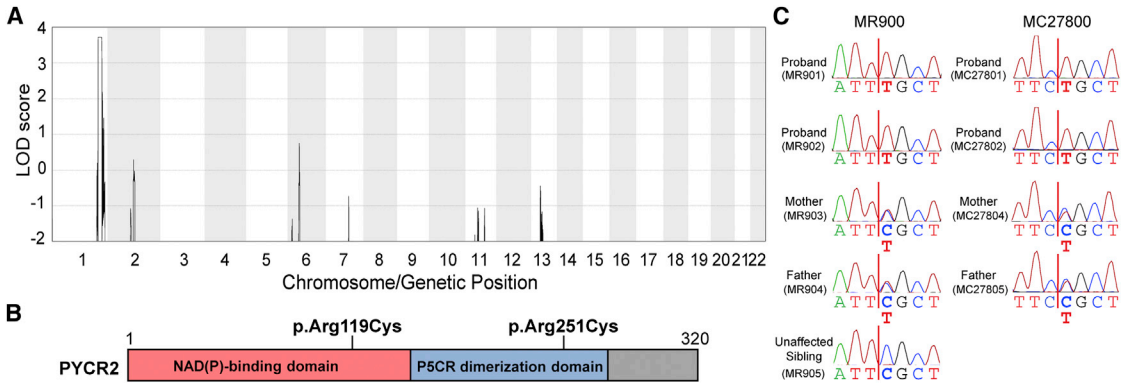

Figure 2. Linkage Mapping and Identification of *PYCR2* Mutations
(A) Genome-wide LOD scores combined for the two families show the only significant linkage region to be 1q42, which has a maximum multipoint LOD score of 3.72.
(B) Schematic representation of the PYCR2 variants. Residue Arg119 is in the NAD(P)-binding domain, and residue Arg251 is in the dimerization domain.
(C) Sanger sequencing confirmed the identified variants in family MR900 (c.355C>T [p.Arg119Cys]) and family MC27800 (c.751C>T [p.Arg251Cys]). These variants segregated with the disease phenotype in each family. Positions of variants are according to RefSeq NM_013328.3 (cDNA) and RefSeq NP_037460.2 (protein).

PolyPhen-2,[22] SIFT,[23] and PROVEAN,[24] suggesting their pathogenicity (Table S3). We also searched for additional deleterious *PYCR2* alleles in our database of 82 exomes from individuals with microcephaly, but we did not find other convincing disease-causing mutations.

Expression of *PYCR2* in the Developing Human Brain

To understand the function of PYCR2 in the human brain, we first analyzed RNA sequencing data of fetal human brain at Carnegie stage 18. We found that *PYCR2* mRNA was moderately expressed in the developing human brain (Figure S1) and that its level of expression was much greater than that of *PYCR1* (MIM 179035) and *PYCRL*, genes encoding PYCR2 isozymes.

PYCR2 Variants Lead to Reduced PYCR2 Levels

We established a lymphoblastoid cell line from one of the affected individuals (MR901) with the homozygous p.Arg119Cys variant and performed immunoblot analysis of PYCR2. The PYCR2 level was markedly lower in this cell line than in a control cell line (Figures 3A and 3B). In order to further assess the effect of the *PYCR2* variants that we identified, we transfected HEK293FT cells with wild-type and mutant *PYCR2* cDNA and measured the resulting PYCR2-V5 levels. Compared to cells transfected with wild-type *PYCR2*, cells transfected with mutant *PYCR2* showed a marked decrease in the amount of variant protein with the p.Arg119Cys substitution and a small decrease in the amount of variant protein with the p.Arg251Cys substitution (Figure 3C). This was confirmed quantitatively by immunoblot analysis, in which the PYCR2-V5/EGFP intensity ratios were measured to adjust for transfection efficiency (Figures 3D and 3E).

Because residue Arg251 is in the dimerization domain, we also performed a co-immunoprecipitation assay to test whether the variant p.Arg251Cys would affect homodimerization of PYCR2. Wild-type HEK293FT cells were transfected with both HA-tagged and V5-tagged *PYCR2* cDNA (wild-type or c.751C>T mutant, which encodes p.Arg251Cys). The lysates were immunoprecipitated with anti-HA antibody beads and were blotted with anti-HA and anti-V5 antibodies. Wild-type PYCR2 showed an abundant signal with anti-V5 antibody, suggesting robust homodimerization. The p.Arg251Cys variant PYCR2 also showed a strong signal with anti-V5 antibody, though to a lesser extent (Figure S2). These data suggest that the p.Arg251Cys variant does not completely abolish the ability of PYCR2 to form a homodimer.

Human PYCR2 Localizes to Mitochondria

To investigate the cellular function of PYCR2, we created a PYCR2-deficient HEK293FT cell line by using the CRISPR-Cas9 system. We introduced a homozygous, 1-bp insertion expected to lead to a frameshift and premature truncation (c.737_738insA [p.Ser247Glufs*13]; Figure S3A) into the *PYCR2* coding region. Immunoblot analysis of fractionated lysates from wild-type and mutant HEK293FT cells revealed that endogenous PYCR2 localized to the mitochondrial fraction in wild-type cells but was absent from mutant cells (Figure S3B). Immunocytochemistry of wild-type and mutant cells similarly showed that PYCR2 localized to mitochondria in wild-type cells, whereas the level of PYCR2 was negligible in cells with mutant *PYCR2* (Figure S3C). Of note, MitoTracker, the membrane-potential-dependent mitochondrial marker used, displayed markedly weaker staining in cells with mutant *PYCR2*. Mitochondrial localization of PYCR2 was also confirmed by transfection of *PYCR2* cDNA (Figure S4). Both the p.Arg119Cys and p.Arg251Cys variant PYCR2 proteins also localized to mitochondria, but interestingly the MitoTracker signal was also much weaker when the mutant cDNAs were transfected.

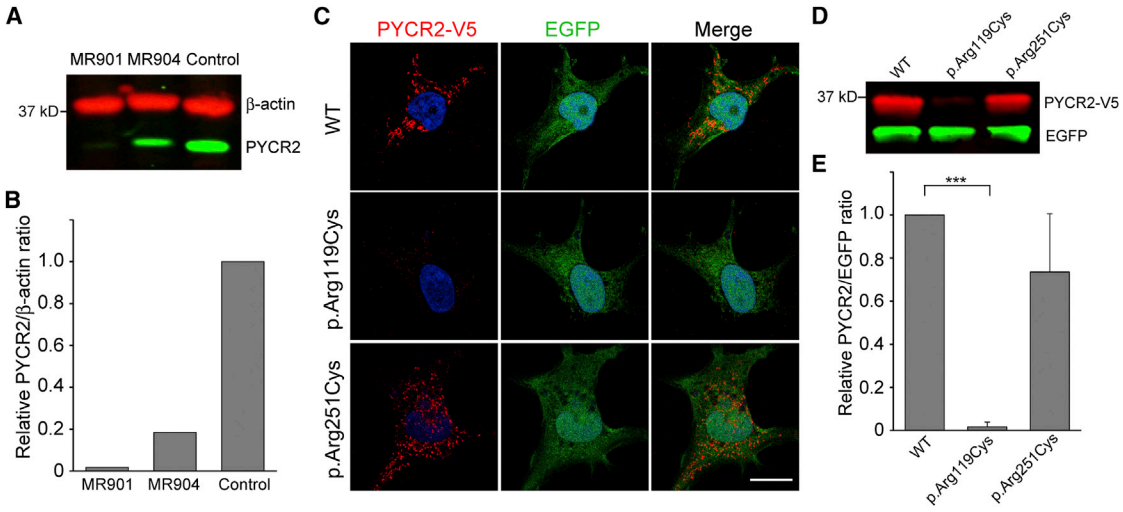

Figure 3. Effect of *PYCR2* Mutations

(A) Immunoblot analysis of PYCR2 levels in lymphoblastoid cell lines. Cells from an affected individual (MR901) showed a marked reduction of PYCR2, whereas cells from his father (MR904) showed a mild reduction.

(B) Quantification of PYCR2 levels. The PYCR2/β-actin intensity ratios for MR901 and MR904 were measured in relation to that of the control subject.

(C) Abundance of wild-type (WT) and variant (p.Arg119Cys and p.Arg251Cys) PYCR2 in transfected HEK293FT cells. The cells were transfected with a wild-type or mutant human *PYCR2* cDNA construct with a C-terminal V5 tag, along with a separate EGFP construct. Immunostaining for V5 showed an almost undetectable level of the p.Arg119Cys variant protein and mildly decreased level of the p.Arg251Cys variant protein. The scale bar represents 20 μm.

(D) Immunoblot analysis of PYCR2 and EGFP levels in transfected HEK293FT cells showed a dramatic reduction of the p.Arg119Cys variant protein and a mild reduction of the p.Arg251Cys variant protein. EGFP served as a transfection control.

(E) Immunoblot analysis was quantified by comparison of the PYCR2-V5/EGFP intensity ratio between the variants proteins and the wild-type protein. The data were averaged from three independent experiments. The p.Arg119Cys variant showed less than 2% of the wild-type abundance. Although the p.Arg251Cys variant did not reach statistical significance, it showed a trend toward abundance lower than wild-type abundance. Error bars represent the SD. ***$p < 0.001$.

Given the role of PYCR2 in proline biosynthesis, we sought to investigate whether the PYCR2-deficient cells would show defective protein synthesis in mitochondria. Thus, in wild-type and PYCR2-deficient cells, we measured the abundance of two components of the oxidative phosphorylation enzyme complex, MT-CO2 and SDHA, which are encoded by mitochondrial DNA and nuclear DNA, respectively. Immunoblotting revealed that there was no significant difference in the abundance of these proteins between wild-type and PYCR2-deficient cells, suggesting that loss of PYCR2 does not lead to a gross defect in mitochondrial protein synthesis (Figure S5).

Loss of Function of PYCR2 Leads to Increased Apoptosis under Oxidative Stress

Progressive microcephaly and reduced white matter in the affected individuals reported herein could suggest ongoing cell death in the CNS. Considering that mitochondria have been implicated in the regulation of apoptosis (reviewed in Wang and Youle[25]), we sought to test the possibility that the loss of PYCR2 function might impair this regulation by performing a TUNEL assay with wild-type HEK293FT cells and the CRISPR-Cas9-engineered PYCR2-deficient cells. TUNEL staining revealed no significant difference in apoptosis between the wild-type and PYCR2-deficient cell lines under normal culture conditions (data not shown). However, 1 hr of incubation in 400 μM hydrogen peroxide led to more TUNEL-positive cells in the mutant cell lines than in wild-type cells (Figures 4A and 4B), indicating that PYCR2 is involved in the cell's response to oxidative stress.

Zebrafish Morpholino Knockdown of a *PYCR2* Ortholog Recapitulates Human Microcephaly

To investigate the role of PYCR2 during brain development, we performed zebrafish gene-knockdown experiments targeting *PYCR2* orthologs. *PYCR2* has two zebrafish orthologs, *pycr1a* (RefSeq NM_200826.1) and *pycr1b* (RefSeq NM_001020618.1), and they share comparable homology to human *PYCR2*. We first attempted to knock down each of *pycr1a* and *pycr1b* by using MOs. Knockdown of *pycr1b* resulted in a small head, whereas knockdown of *pycr1a* led to a previously described skin phenotype (loosening of epidermis),[21] but the effect on the head size was less noticeable. Therefore, we focused subsequent analysis on *pycr1b*.

When embryos were injected with 3.5 ng of the *pycr1b* MO, approximately one-third of the morphant larvae at 4 dpf appeared severely affected by a small head and eyes, short body, a down-tilted tail, and hypomotility, whereas nearly two-thirds of the morphants showed a milder phenotype of a small head and eyes and hypomotility (Figure 5A and Figure S6). These phenotypic effects were dose dependent. Small head size was evident by

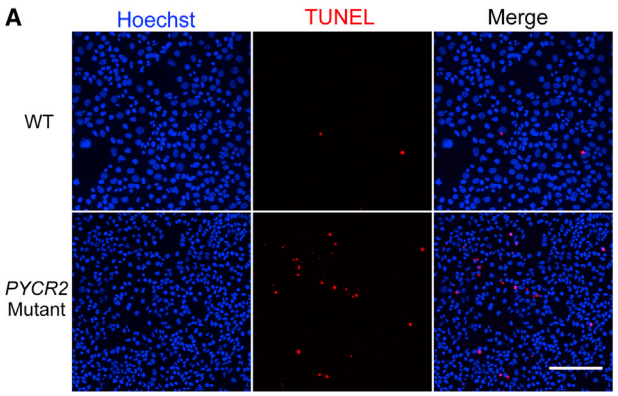

Figure 4. PYCR2 Loss of Function Increases Apoptosis under Oxidative Stress
(A) HEK293FT cells were treated with 400 μM H_2O_2 for 1 hr, followed by 24 hr in culture. The mutant cells, harboring a homozygous frameshift mutation (*PYCR2* mutant), showed more apoptosis than did wild-type cells, as detected by TUNEL assay. The scale bar represents 200 μm.
(B) Quantification of TUNEL assay revealed a statistically significant increase in apoptosis of the mutant cells treated with H_2O_2. Data were averaged from two independent experiments. Error bars represent the SD. **$p < 0.01$.

1 dpf (Figures S7A and S7B) and became more obvious at later stages. The maximum head width measured for morphant larvae at 4 dpf was significantly smaller than that of controls (Figures 5A and 5B). Histological sections of the brains of morphant larvae were consistent with a smaller brain size affecting the forebrain, midbrain, and hindbrain (Figures 5C and 5D). There were no obvious skin defects observed in *pycr1b* morphants.

Finally, we performed rescue experiments with human *PYCR2* mRNA. When wild-type human *PYCR2* mRNA was co-injected with the *pycr1b* MO, the microcephaly phenotype was rescued (Figures 5A and 5B and Figure S7C). On the other hand, almost no rescue was observed with human *PYCR2* mRNA harboring the c.355C>T variant, and only partial rescue was noted with the c.751C>T variant (Figure 5B). These results further support the pathogenicity of the identified *PYCR2* variants.

Discussion

Herein, we have shown that mutations in *PYCR2*, which encodes an enzyme in the proline biosynthesis pathway, lead to a phenotype of microcephaly with cerebral hypomyelination in humans. In four affected individuals from two unrelated consanguineous families, we identified two mutant *PYCR2* alleles that are predicted to affect protein function. We took advantage of the newly developed CRISPR-Cas9 system to generate a cellular model of PYCR2 loss of function and showed that deficiency of PYCR2 resulted in increased apoptosis under oxidative stress. Knockdown of a zebrafish *PYCR2* ortholog, *pycr1b*, recapitulated the microcephaly phenotype, which was rescued by wild-type human *PYCR2* mRNA, but not by mRNAs harboring the human mutations. Together, these results support the pathogenicity of the identified *PYCR2* mutations and suggest that mitochondria-induced apoptosis in the CNS is a potential mechanism for microcephaly in these affected individuals.

PYCR2 is one of three human pyrroline-5-carboxylate reductases (PYCRs) that catalyze the reduction of Δ1-pyrroline-5-carboxylate (P5C) to proline while oxidizing NAD(P)H to $NAD(P)^+$.[26,27] We showed that the two identified variants in PYCR2 occur at highly conserved amino acids and that the levels of the altered proteins were lower in transfected cells, suggesting that these two variants affect the stability of the resulting PYCR2.

Several genetic disorders affecting proline biosynthesis have been described. Interestingly, mutations in *PYCR1*, encoding an isozyme of PYCR2, cause autosomal-recessive cutis laxa with progeroid features, including autosomal-recessive cutis laxa type IIB (MIM 612940) and type IIIB (MIM 614438).[21] Of note, some of the reported pathogenic PYCR1 variants are at Arg119 and Arg251, the residues corresponding to the mutated regions in *PYCR2* in the individuals described herein. The clinical features of individuals with *PYCR1* mutations include wrinkled skin, joint hyperlaxity, characteristic facial features including a triangular face, short nose, long philtrum, and large ears, mild to moderate microcephaly, and psychomotor retardation.[28] Although information on brain-imaging findings is limited, some individuals with *PYCR1* mutations have been reported to have an abnormal corpus callosum and enlarged ventricles, but abnormalities of myelination have not been reported.[29,30] In contrast, individuals affected by *PYCR2* mutations do not present with cutis laxa and show evidence of significant hypomyelination on brain MRI. There is some phenotypic overlap between *PYCR1* and *PYCR2* mutations in terms of microcephaly and global developmental delay, as well as joint hyperlaxity, which was noted only in family MC27800. However, they seem to cause clinically distinct conditions, and mutations in *PYCR2* appear to lead to a syndrome of microcephaly and hypomyelination.

The different phenotypes caused by the PYCR1 and PYCR2 variants suggest that each of these isozymes has a unique role in the human body. Both PYCR1 and PYCR2 are thought to localize to mitochondria and primarily act in the conversion of glutamate to proline.[26] Another isozyme, PYCRL, is thought to localize to the cytosol and primarily be involved in converting ornithine to proline. We observed that *PYCR2* mRNA was more highly expressed than *PYCR1* and *PYCRL* in the developing human brain, and so different spatial and temporal expression patterns

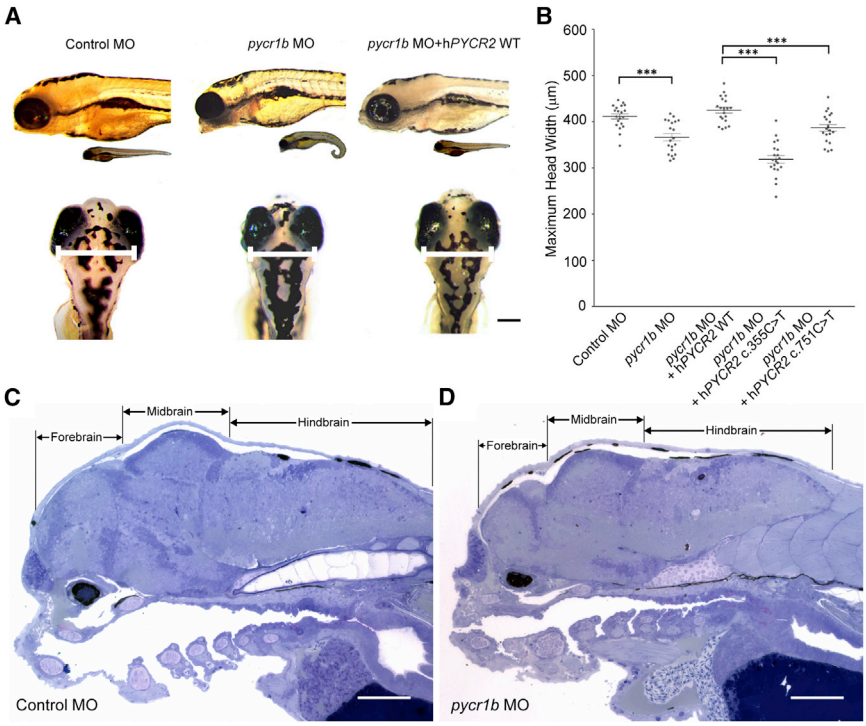

Figure 5. Morpholino-Based Knockdown of Zebrafish *pycr1b* Recapitulates the Human Microcephaly Phenotype

(A) Compared to zebrafish injected with control MO (control MO), 4-dpf zebrafish larvae injected with 3.5 ng *pycr1b* MO at the 1- to 2-cell stage (*pycr1b* MO) showed a small head size (horizontal white bars represent the maximum head width measured) and a curved tail. Co-injection of human *PYCR2* mRNA (h*PYCR2* WT; 20 pg) rescued the phenotype. The scale bar represents 100 μm. Representative images are shown.

(B) Measurements of the maximum head width of *pycr1b* morphants were significantly smaller than those of the control. Co-injection of human *PYCR2* mRNA (h*PYCR2* WT) rescued the phenotype, but mutant mRNAs (h*PYCR2* c.355C>T and h*PYCR2* c.751C>T) failed to show a full rescue effect. Twenty larvae for each category were randomly selected for measurement of the maximum head width illustrated in (A). Bars represent the mean value and SEM. ***$p < 0.001$.

(C and D) Sagittal brain sections of larvae injected with control MO (C) or *pycr1b* MO (D) at 4 dpf were stained with toluidine blue. The size of the forebrain, midbrain, and hindbrain was significantly smaller in the *pycr1b* morphant than in the control. Scale bars represent 100 μm.

could in part explain the differences in the resulting clinical phenotypes. However, there might be other biological reasons for the distinct phenotypes. For example, enzymatic properties of PYCR1 and PYCR2 have been reported to be different: PYCR2 has been shown to be more catalytically efficient than PYCR1 in the presence of NADH, and at the same time, PYCR2 has been shown to be more susceptible to product inhibition.[26] Thus, PYCR1 and PYCR2 could play overlapping, yet non-redundant roles in mitochondrial physiology.

Although PYCR2 is an enzyme for proline biosynthesis, systemic deprivation of proline does not appear to be the pathogenetic mechanism of this condition, given that plasma amino acid analysis in two affected individuals did not show low proline levels. Furthermore, we showed that mitochondrial protein synthesis was not affected in PYCR2-deficient cells. Therefore, deficiency of proline, as a building block of proteins, might not be the major pathophysiology. However, proline has been reported as a non-enzymatic antioxidant that suppresses apoptosis,[31] and therefore local proline biosynthesis in neurons might be important for neuronal protection against oxidative stress. In the current study, we demonstrated that engineered PYCR2-deficient cells displayed significantly more apoptosis than wild-type cells under oxidative stress, suggesting the involvement of PYCR2 in the cellular response to oxidative stress. In addition, a membrane-potential-dependent mitochondrial marker displayed much weaker staining in the PYCR2-deficient cells, indicating that PYCR2 is essential in maintaining mitochondrial membrane potential. It is also important to note that the reaction catalyzed by PYCRs leads to both a reduction of P5C to proline and oxidation of NAD(P)H to NAD(P)+, and so PYCRs might also be involved in regulating NAD(P)H and NAD(P)+, molecules that have been implicated in neuronal cell death (reviewed in Ying[32]).

The pathogenesis of hypomyelination in the individuals with *PYCR2* mutations is not immediately clear. Previously reported genes mutated in conditions with hypomyelination encode proteins with diverse functions, but they do not obviously share biological pathways with PYCR2. Myelination is an energy-expensive process, and energy deprivation negatively affects oligodendrocyte development and myelination.[33] In addition, involvement of cerebral white matter can be seen in individuals with mitochondrial encephalopathies.[34] Therefore, energy failure in oligodendrocytes is one plausible mechanism.

In summary, we identified mutations in *PYCR2* as the cause of a genetic disorder characterized by microcephaly and hypomyelination. We demonstrated that PYCR2-deficient cells showed increased apoptosis under oxidative stress, and therefore postnatal microcephaly in affected individuals is most likely due to increased cell death in the CNS.

Supplemental Data

Supplemental Data include seven figures and three tables and can be found with this article online at http://dx.doi.org/10.1016/j.ajhg.2015.03.003.

Acknowledgments

The study was supported by grants from the Manton Center for Orphan Disease Research, National Institute of Neurological Disorders and Stroke (NINDS, R01NS035129), NIH Fogarty International Center (R21TW008223), and the Dubai Harvard Foundation for Medical Research. T.N. was supported by fellowship grants from the Japan Foundation for Pediatric Research and the Japan Epilepsy Research Foundation. A.P. was supported by the NINDS (1K23 NS069784) and the Boston Children's Hospital Translational Research Program. G.H.M. was also supported by grants from F. Hoffmann-La Roche, the Qatar National Research Fund, and the Boston Children's Hospital Faculty Career Development Award. Human embryonic material was provided by the joint Medical Research Council and Wellcome Trust (grant 099175/Z/12/Z) Human Developmental Biology Resource (www.HDBR.org). We thank the families for their participation in this research, Dr. Gilad D. Evrony for help with RNA sequencing, Dr. Xiaochang Zhang, Dr. Aldo Rozzo, Dr. Byoung-Il Bae, Ms. Rachel E. Reiff, and Dr. Anthony D. Hill for technical assistance, and Dr. Christopher A. Walsh and Dr. Gerard T. Berry for helpful discussions and critical comments on the manuscript.

Received: December 13, 2014
Accepted: March 5, 2015
Published: April 9, 2015

Web Resources

The URLs for data presented herein are as follows:
1000 Genomes, http://www.1000genomes.org/
ANNOVAR, http://www.openbioinformatics.org/annovar/
Burrows-Wheeler Aligner, http://bio-bwa.sourceforge.net
Complete Genomics 69 Genomes Data, http://www.completegenomics.com/public-data/69-Genomes/
dbSNP, http://www.ncbi.nlm.nih.gov/SNP/
GATK, http://www.broadinstitute.org/gatk/
ImageJ, http://imagej.nih.gov/ij/
InterPro, http://www.ebi.ac.uk/interpro/
MERLIN, http://csg.sph.umich.edu/abecasis/Merlin/
NHLBI Exome Sequencing Project (ESP) Exome Variant Server, http://evs.gs.washington.edu/EVS/
OMIM, http://www.omim.org
Picard, http://broadinstitute.github.io/picard/
PLINK, http://pngu.mgh.harvard.edu/purcell/plink/
PolyPhen-2, http://genetics.bwh.harvard.edu/pph2/
Primer3, http://primer3.ut.ee/
PROVEAN, http://provean.jcvi.org
RefSeq, http://www.ncbi.nlm.nih.gov/RefSeq
SAMtools, http://samtools.sourceforge.net/
SIFT, http://sift.jcvi.org

References

1. Ashwal, S., Michelson, D., Plawner, L., and Dobyns, W.B.; Quality Standards Subcommittee of the American Academy of Neurology and the Practice Committee of the Child Neurology Society (2009). Practice parameter: Evaluation of the child with microcephaly (an evidence-based review): report of the Quality Standards Subcommittee of the American Academy of Neurology and the Practice Committee of the Child Neurology Society. Neurology *73*, 887–897.
2. Mochida, G.H., and Walsh, C.A. (2001). Molecular genetics of human microcephaly. Curr. Opin. Neurol. *14*, 151–156.
3. Sahai, I., Mochida, G.H., Grabowski, E.F., and Caruso, P.A. (2014). Case records of the Massachusetts General Hospital. Case 27-2014. A 10-month-old boy with microcephaly and episodic cyanosis. N. Engl. J. Med. *371*, 847–858.
4. Bond, J., Roberts, E., Mochida, G.H., Hampshire, D.J., Scott, S., Askham, J.M., Springell, K., Mahadevan, M., Crow, Y.J., Markham, A.F., et al. (2002). ASPM is a major determinant of cerebral cortical size. Nat. Genet. *32*, 316–320.
5. Yu, T.W., Mochida, G.H., Tischfield, D.J., Sgaier, S.K., Flores-Sarnat, L., Sergi, C.M., Topçu, M., McDonald, M.T., Barry, B.J., Felie, J.M., et al. (2010). Mutations in WDR62, encoding a centrosome-associated protein, cause microcephaly with simplified gyri and abnormal cortical architecture. Nat. Genet. *42*, 1015–1020.
6. Shen, J., Gilmore, E.C., Marshall, C.A., Haddadin, M., Reynolds, J.J., Eyaid, W., Bodell, A., Barry, B., Gleason, D., Allen, K., et al. (2010). Mutations in PNKP cause microcephaly, seizures and defects in DNA repair. Nat. Genet. *42*, 245–249.
7. Pouwels, P.J., Vanderver, A., Bernard, G., Wolf, N.I., Dreha-Kulczewksi, S.F., Deoni, S.C., Bertini, E., Kohlschütter, A., Richardson, W., Ffrench-Constant, C., et al. (2014). Hypomyelinating leukodystrophies: translational research progress and prospects. Ann. Neurol. *76*, 5–19.
8. van der Knaap, M.S., Breiter, S.N., Naidu, S., Hart, A.A., and Valk, J. (1999). Defining and categorizing leukoencephalopathies of unknown origin: MR imaging approach. Radiology *213*, 121–133.
9. Gencic, S., Abuelo, D., Ambler, M., and Hudson, L.D. (1989). Pelizaeus-Merzbacher disease: an X-linked neurologic disorder of myelin metabolism with a novel mutation in the gene encoding proteolipid protein. Am. J. Hum. Genet. *45*, 435–442.
10. Hudson, L.D., Puckett, C., Berndt, J., Chan, J., and Gencic, S. (1989). Mutation of the proteolipid protein gene PLP in a human X chromosome-linked myelin disorder. Proc. Natl. Acad. Sci. USA *86*, 8128–8131.
11. Simons, C., Wolf, N.I., McNeil, N., Caldovic, L., Devaney, J.M., Takanohashi, A., Crawford, J., Ru, K., Grimmond, S.M., Miller, D., et al. (2013). A de novo mutation in the β-tubulin gene TUBB4A results in the leukoencephalopathy hypomyelination with atrophy of the basal ganglia and cerebellum. Am. J. Hum. Genet. *92*, 767–773.
12. de Koning, T.J., Jaeken, J., Pineda, M., Van Maldergem, L., Poll-The, B.T., and van der Knaap, M.S. (2000). Hypomyelination and reversible white matter attenuation in 3-phosphoglycerate dehydrogenase deficiency. Neuropediatrics *31*, 287–292.
13. Jaeken, J., Detheux, M., Van Maldergem, L., Foulon, M., Carchon, H., and Van Schaftingen, E. (1996). 3-Phosphoglycerate dehydrogenase deficiency: an inborn error of serine biosynthesis. Arch. Dis. Child. *74*, 542–545.
14. Hyland, K., Smith, I., Bottiglieri, T., Perry, J., Wendel, U., Clayton, P.T., and Leonard, J.V. (1988). Demyelination and decreased S-adenosylmethionine in 5,10-methylenetetrahydrofolate reductase deficiency. Neurology *38*, 459–462.
15. Purcell, S., Neale, B., Todd-Brown, K., Thomas, L., Ferreira, M.A., Bender, D., Maller, J., Sklar, P., de Bakker, P.I., Daly, M.J., and Sham, P.C. (2007). PLINK: a tool set for whole-genome association and population-based linkage analyses. Am. J. Hum. Genet. *81*, 559–575.

16. Abecasis, G.R., Cherny, S.S., Cookson, W.O., and Cardon, L.R. (2002). Merlin—rapid analysis of dense genetic maps using sparse gene flow trees. Nat. Genet. *30*, 97–101.
17. Reiff, R.E., Ali, B.R., Baron, B., Yu, T.W., Ben-Salem, S., Coulter, M.E., Schubert, C.R., Hill, R.S., Akawi, N.A., Al-Younes, B., et al. (2014). METTL23, a transcriptional partner of GABPA, is essential for human cognition. Hum. Mol. Genet. *23*, 3456–3466.
18. Ran, F.A., Hsu, P.D., Wright, J., Agarwala, V., Scott, D.A., and Zhang, F. (2013). Genome engineering using the CRISPR-Cas9 system. Nat. Protoc. *8*, 2281–2308.
19. Schneider, C.A., Rasband, W.S., and Eliceiri, K.W. (2012). NIH Image to ImageJ: 25 years of image analysis. Nat. Methods *9*, 671–675.
20. Frezza, C., Cipolat, S., and Scorrano, L. (2007). Organelle isolation: functional mitochondria from mouse liver, muscle and cultured fibroblasts. Nat. Protoc. *2*, 287–295.
21. Reversade, B., Escande-Beillard, N., Dimopoulou, A., Fischer, B., Chng, S.C., Li, Y., Shboul, M., Tham, P.Y., Kayserili, H., Al-Gazali, L., et al. (2009). Mutations in PYCR1 cause cutis laxa with progeroid features. Nat. Genet. *41*, 1016–1021.
22. Adzhubei, I., Jordan, D.M., and Sunyaev, S.R. (2013). Predicting functional effect of human missense mutations using PolyPhen-2. Curr. Protoc. Hum. Genet. *Chapter 7*, Unit 7.20.
23. Kumar, P., Henikoff, S., and Ng, P.C. (2009). Predicting the effects of coding non-synonymous variants on protein function using the SIFT algorithm. Nat. Protoc. *4*, 1073–1081.
24. Choi, Y., Sims, G.E., Murphy, S., Miller, J.R., and Chan, A.P. (2012). Predicting the functional effect of amino acid substitutions and indels. PLoS ONE *7*, e46688.
25. Wang, C., and Youle, R.J. (2009). The role of mitochondria in apoptosis. Annu. Rev. Genet. *43*, 95–118.
26. De Ingeniis, J., Ratnikov, B., Richardson, A.D., Scott, D.A., Aza-Blanc, P., De, S.K., Kazanov, M., Pellecchia, M., Ronai, Z., Osterman, A.L., and Smith, J.W. (2012). Functional specialization in proline biosynthesis of melanoma. PLoS ONE *7*, e45190.
27. Phang, J.M., Liu, W., and Zabirnyk, O. (2010). Proline metabolism and microenvironmental stress. Annu. Rev. Nutr. *30*, 441–463.
28. Dimopoulou, A., Fischer, B., Gardeitchik, T., Schröter, P., Kayserili, H., Schlack, C., Li, Y., Brum, J.M., Barisic, I., Castori, M., et al. (2013). Genotype-phenotype spectrum of PYCR1-related autosomal recessive cutis laxa. Mol. Genet. Metab. *110*, 352–361.
29. Guernsey, D.L., Jiang, H., Evans, S.C., Ferguson, M., Matsuoka, M., Nightingale, M., Rideout, A.L., Provost, S., Bedard, K., Orr, A., et al. (2009). Mutation in pyrroline-5-carboxylate reductase 1 gene in families with cutis laxa type 2. Am. J. Hum. Genet. *85*, 120–129.
30. Yildirim, Y., Tolun, A., and Tüysüz, B. (2011). The phenotype caused by PYCR1 mutations corresponds to geroderma osteodysplasticum rather than autosomal recessive cutis laxa type 2. Am. J. Med. Genet. A. *155A*, 134–140.
31. Chen, C., and Dickman, M.B. (2005). Proline suppresses apoptosis in the fungal pathogen Colletotrichum trifolii. Proc. Natl. Acad. Sci. USA *102*, 3459–3464.
32. Ying, W. (2007). NAD+ and NADH in neuronal death. J. Neuroimmune Pharmacol. *2*, 270–275.
33. Yan, H., and Rivkees, S.A. (2006). Hypoglycemia influences oligodendrocyte development and myelin formation. Neuroreport *17*, 55–59.
34. Moroni, I., Bugiani, M., Bizzi, A., Castelli, G., Lamantea, E., and Uziel, G. (2002). Cerebral white matter involvement in children with mitochondrial encephalopathies. Neuropediatrics *33*, 79–85.